EURASIP Journal on Applied Signal Processing 2005:3, 346–358

A New Time-Hopping Multiple Access Communication System Simulator: Application to Ultra-Wideband

Galo Nuño-Barrau
Departamento de Señales, Sistemas y Radiocomunicaciones, Universidad Politécnica de Madrid, 28040 Madrid, Spain
Email: galo@gaps.ssr.upm.es

José M. Páez-Borrallo
Departamento de Señales, Sistemas y Radiocomunicaciones, Universidad Politécnica de Madrid, 28040 Madrid, Spain
Email: jmpaez@etsit.upm.es

Received 14 September 2003; Revised 16 May 2004

Time-hopping ultra-wideband technology presents some very attractive features for future indoor wireless systems in terms of achievable transmission rate and multiple access capabilities. This paper develops an algorithm to design time-hopping system simulators specially suitable for ultra-wideband, which takes advantage of some of the specific characteristics of this kind of systems. The algorithm allows an improvement of both the time capabilities and the achievable sampling rate and can be used to research into the influence of different parameters on the performance of the system. An additional result is the validation of a new general performance formula for time-hopping ultra-wideband systems with multipath channels.

Keywords and phrases: ultra-wideband, time hopping, WPAN, spread spectrum, multipath channel, simulation.

1. INTRODUCTION

Multiple access (MA) systems based on time-hopping spread-spectrum (TH-SS) techniques have recently started to be taken into consideration as a possible solution for the implementation of the future short-range personal communication systems (PCSs) or wireless personal area networks (WPANs) [1]. So far, the most important TH-SS system has been time-hopping ultra-wideband (TH-UWB), which is characterized by the use of signals with very large relative bandwidths and reduced power spectral densities [2, 3]. According to the US Federal Communications Commission's (FCC) first report and order, an UWB device can be defined as any device emitting radio signals with a -10 dB fractional bandwidth greater than 0.2 or a bandwidth of at least 500 MHz at all times of transmission [4]. In TH-UWB, this can be achieved by the pseudorandom transmission of very narrow signals, usually referred to as monocycles or monopulses [5].

TH-UWB presents some characteristics that make these systems very attractive for high-speed WPAN as 802.15.3 or indoor communications [6, 7], such as the possibility of resolving dense multipath interference (a consequence of the extremely high delay resolution of the signals), low consumption, high resistance to the interference from other communication systems, low probability of interception, high spatial resolution or the possibility of coexistence with other radio systems in the same frequency bands. After the FCC ruling in February 2003, the development of UWB technology has been accelerated by the entry of new enterprises and research centers that are providing new approaches to solve some of the main problems of UWB systems.

In order to design a real TH-UWB system, many aspects should be taken into careful consideration, such as modulation schemes, waveforms design, time-hopping codes, receiver architecture, decision schemes, or channel models, most of them are under discussion at the present moment. Therefore, to develop accurate and flexible simulation tools is necessary to analyze the influence of these factors and to have a deeper perspective of the performance of the system before a physical prototype can be constructed. Unfortunately, the development of a software simulator for UWB has several difficulties derived from the extremely large sampling rate necessary to process these ultra-wide bandwidth signals. In a straightforward approach with a constant sampling rate, the length of the array that contains the samples of a single bit can be very large, depending on the relationship between the duty cycle and the bit and chip rates. This array should

pass through different blocks that model the channel and the receiver responses; so a considerable number of operations should be made and consequently the total computing time is very high, even in very fast workstations.

Some simulators presented in the literature try to avoid this problem by using variable-rate sampling [8]. However, in channels with a considerable number of multipath components and several users, the necessary computational requirements to evaluate and process the possible overlapping between the desired windows and the interfering signals produce high simulation times, specially for low bit error rates (BERs). This fact reduces considerably the efficiency.

In this paper, a new method to design a TH-UWB (or in general TH) communication system simulator is presented. The method takes advantage of some of the properties of this kind of systems in order to provide a very straightforward and fast processing that improves all the previous designs by several orders of magnitude, independently of the sampling rate (which can reach some tens of gigasamples per second) and flexible enough to admit all the different characteristics mentioned above (modulation, channels, sequences, etc.). As an application of the use of the simulator, a new theoretical formula to predict the system performance has been validated, based on the one presented in [2].

This paper is organized as follows. In Section 2, a complete mathematical model of a TH system is presented based on the previous research found in the literature. From this model, in Section 3, it is shown how changes can be made in the signal processing to allow the development of an enhanced linear algorithm to simulate the whole system. Finally, in Section 4, numerical results are provided under different sets of parameters to analyze the simulator performance, including a comparison with other simulators presented in the literature and the validation of the new performance formula.

2. GENERAL MODEL OF A UWB COMMUNICATIONS SYSTEM

2.1. Signal description

We consider a UWB system composed of N_u different links. These links can correspond to different real users transmitting and receiving through different terminals or to different links established between two terminals in order to achieve a higher aggregate bit rate. No further assumptions about the symmetry of these links will be made, so they can be symmetric or asymmetric depending on the system functionality (file downloading, video streaming, videoconference, telemetry, etc.). In the case of different terminals, they can be static or mobile and they can be close to one another or relatively far apart, taking into account that so far the main applications of this kind of systems are indoor communications, where distances cannot be too large.

The transmitted signal in one direction of one of the links consists of a series of pulses whose frame structure can be seen in Figure 1. A single bit is composed of N_s chips, each of them with period T_f. Each one of the chips is subdivided into

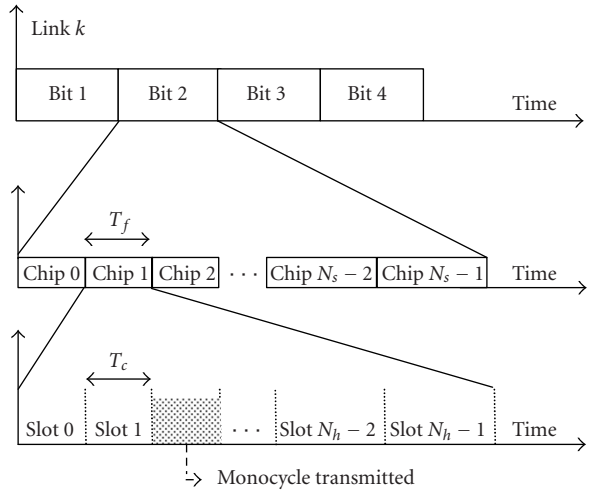

Figure 1: Frame structure for TH signals.

N_h slots of length T_c. The monocycle is transmitted in one of these slots (one monocycle per chip), in a position (number of the slot) given by a pseudorandom TH sequence. The data modulation in the monocycles can be in amplitude, phase, or time shift, and the slot length T_c must be large enough to contain the different monocycles.

The bit rate is $1/T_f N_s$ or equivalently $1/T_c N_h N_s$. In [9], an M-ary scheme is also proposed, where instead of coding single bits, it is possible to code groups of bits using M-ary monocycle alphabets. In this case, instead of bits, groups of $\log_2(M)$ bits are transmitted in each symbol (which would be divided into N_s chips with N_h slots each one). This method allows an increment in the bit rate but the receiver complexity can make it unsuitable for this kind of systems.

Given the kth link, the signal transmitted at the connection point between the modulator and the antenna has the following structure:

$$s^{(k)}(t) = \sum_{j=-\infty}^{\infty} A a_j^{(k)} w_{\mathrm{tr}}\left(t - jT_f - c_j^{(k)} T_c - d_j^{(k)} \lambda - \tau_0^{(k)}\right), \quad (1)$$

which is an improved version of the one presented in [2]. The meaning of the terms is explained in the following points.

(i) $w_{\mathrm{tr}}(t)$ is the transmitted monocycle. In [10, 11], some possible waveforms for the UWB monocycle have been proposed, such as the first, second, and third derivatives of the Gaussian pulse, the Laplacian pulse, the rectangle pulse, or even one period of a sine wave. Moreover, $w_{\mathrm{tr}}(t)$ can be baseband, as proposed in [3], high pass or modulated, to comply with FCC regulation.

In Figure 2, the waveform of a modulated version of the second derivative of the Gaussian pulse is shown. The modulation itself is different from "classical" narrowband systems, where the carrier frequency is very high related to the signal bandwidth. In UWB systems, the envelope contains only some periods of the carrier in order to keep a high relative bandwidth.

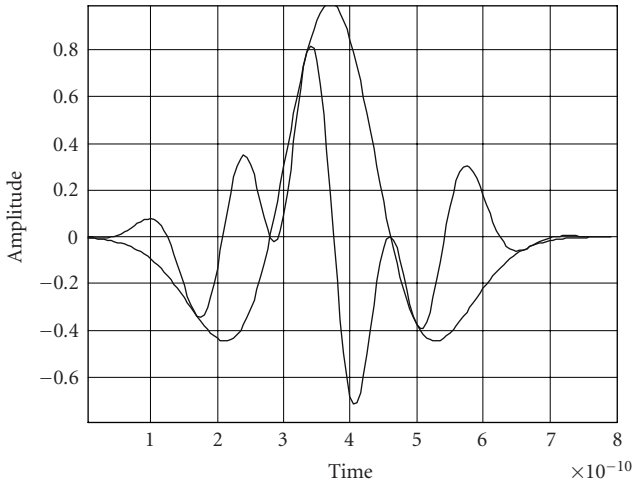

Figure 2: Example of the modulated second derivative of the Gaussian monocycle. The presence of only 5-carrier periods should be noticed.

(ii) T_f is the frame time or chip period, divided in N_h slots of length T_c as it has been previously explained.

(iii) The pseudorandom TH code $\{c_j^{(k)}\}$ is a sequence of integers with period N_p whose values are taken from the range between 0 and $C_{\max}$, with $C_{\max} < N_h$. The integer $c_j^{(k)}$ denotes the slot of the jth chip where the monocycle should be transmitted. In [12], an algorithm to easily design these sequences can be found, and in [13, 14], there are complete analyses of the influence of the codes on the power spectral density (PSD) of the signal.

(iv) The asynchronism between different links is shown by $\tau_0^{(k)}$ as a delay with respect to the beginning of the frame for the first link (from now on, the first link will be considered as the desired signal, and the other links as interference), as represented in Figure 3.

(v) *Pulse-amplitude modulation (PAM)*. $\{a_j^{(k)}\}$ is a sequence of symbols taken from an M-ary alphabet (typically binary) related to the data sequence to be transmitted by the kth link. Depending on the coding scheme, the sequence $\{a_j^{(k)}\}$ can be constant for all the N_s chips or more complicated intrabit codes can be applied to provide an additional error protection. The symbols are scaled by the amplitude constant A. The problem of this modulation scheme is that pulse inversion can happen due to the reflections, and that is the reason why it was not considered in [2]. Notwithstanding, some manufacturers have proposed a binary antipodal PAM as the modulation scheme for UWB systems.

(vi) *Pulse-position modulation (PPM)*. Equivalently, the sequence $\{d_j^{(k)}\}$ can be employed as a sequence of time shifts in a PPM modulation. In [9], a complete analysis of a TH-UWB spread-spectrum MA system based on an M-ary PPM modulation is presented, where M different time shifts are applied to the signals. However, even with the advantages derived from the use of modulation with M greater than 2, the receiver complexity to handle the severe timing requirements

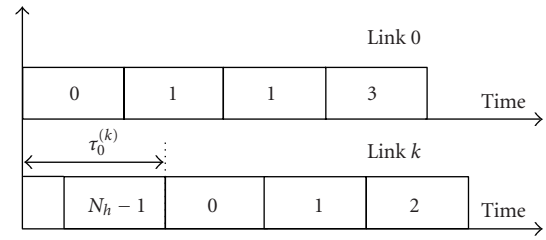

Figure 3: Example of the asynchronism between different links.

can make it completely unsuitable in the practice. This could be the reason why most of the work regarding UWB considers just a binary PPM modulation with a delay constant λ as in [2]. In [15], an alternative intrabit coding based on superorthogonal codes is described that allows the improvement of the bit error probability (BEP) or the increase of the number of links by a factor that is logarithmic with the number of pulses N_s.

The slot length T_c must be greater than the monocycle duration plus the maximum delay due to the PPM modulation in order to be able to contain all the possible signals of the alphabet.

The aim of the modulation is not only the data transmission but also the spectral shaping. An accurate analysis of the influence of data modulation and TH codes, as the one presented in [13], has shown that the combination of PPM and PAM modulations can yield a lower PSD than each of them separately. Therefore, the possibility of combining both schemes should also be taken into careful consideration, not only with the purpose of increasing the data rate but also to lower the PSD, which is crucial in this kind of systems (especially after restrictive FCC ruling).

In Figure 4, a conceptual model of the generation of the signal in (1) is presented. Signal $\Pi(t)$ is defined as

$$\Pi(t) = \sum_{j=-\infty}^{\infty} A a_j^{(k)} \delta\left(t - jT_f - c_j^{(k)} T_c - d_j^{(k)} \lambda - \tau_0^{(k)}\right), \quad (2)$$

where $\delta(t)$ is the Dirac distribution. This signal is introduced in a filter whose impulse response is the shape of the desired monocycle $w_{\text{tr}}(t)$, whose output $s^{(k)}(t)$ is transmitted to the channel.

2.2. Channel model

One of the main problems found in the UWB system simulator design is the lack of a well-established channel model for wideband indoor signal propagation. Many propagation measurements and channel models can be found in the literature, but most of them are narrowband in comparison to the extremely wide UWB spectrum, which can go from nearly DC to 11 GHz. Therefore, it is necessary to take accurate measurements of the channel prior to developing a complete mathematical channel model. For the last years, a steadily growing number of new analysis and models have appeared based on different sets of measurements, and probably more will appear before one is internationally adopted.

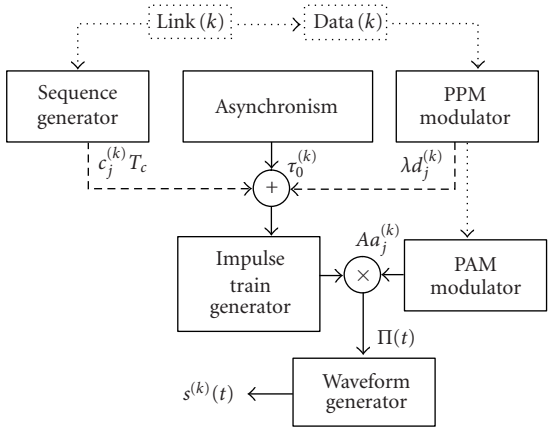

Figure 4: Conceptual model of the UWB signal generation.

As a consequence of that, a TH-UWB simulator should be able to support different channel models with flexibility.

In any wireless channel, the received signal is a sum of the replicas (echoes) of the transmitted signal, being related to the reflecting, absorbing, scattering, and/or deflecting objects via which the signal propagates. There is, however, a major difference between UWB and narrowband systems: in a narrowband system, the echoes at the receiver are only attenuated, phase-shifted, and delayed, but undistorted, so that the received signal may be modeled as a linear combination of L delayed basic waveforms $w_{\text{tr}}(t)$:

$$r^{(k)}(t) = \sum_{l=1}^{L} \beta_l^{(k)} w\left(t - \tau_l^{(k)}\right). \tag{3}$$

In UWB systems, the frequency selectivity of the reflection, absorption, scattering, and/or diffraction coefficients of the objects via which the signal propagates can lead to a distortion or reshaping of the transmitted pulses. Furthermore, the distortion and, thus, the shape of the arriving echoes, varies from echo to echo [16]. The received signal is, thus, given as

$$r^{(k)}(t) = \sum_{l=1}^{L} \beta_l^{(k)}(t)\theta_l\left(t - \tau_l^{(k)}(t)\right), \tag{4}$$

where $\theta_l(t)$ is the received pulse through the lth path.

However, in [16], it is also stated that the distortion of the different propagation paths is negligible in a real situation, so (3) could be considered valid, taking into account a slow variation of both $\beta_l^{(k)}(t)$ and $\tau_l^{(k)}(t)$. Nevertheless, even if this model is very straightforward, it is also too simplistic due to not considering any frequency-depending signal distortion, as the one detected in [17]. Therefore, the impulse response should be

$$r^{(k)}(t) = \sum_{l=1}^{L} \beta_l^{(k)} \theta\left(t - \tau_l^{(k)}\right) \tag{5}$$

that is a particular case of (4) with $\beta_l^{(k)}(t)$ and $\tau_l^{(k)}(t)$ changing slowly in relation to the observation window. Signal distortion is mainly due to antennas radiation and free-space propagation (where higher frequencies are more attenuated) and it can be represented by an impulse response $h_{\text{dist}}(t)$:

$$\theta(t) = w(t) * h_{\text{dist}}(t), \tag{6}$$

where $*$ denotes the convolution product of functions. Therefore, from (5) and (6), a general channel-impulse response $h^{(k)}(t)$ can be represented (for observation windows, where the channel can be considered as static) as

$$h^{(k)}(t) = h_{\text{dist}}(t) * \sum_{l=1}^{L} \beta_l^{(k)} \delta\left(t - \tau_l^{(k)}\right). \tag{7}$$

The received signal will be then a set of pulses distorted by the channel (independently of their paths) with amplitudes depending both on a random distribution to include the different reflection, scattering, and/or diffraction phenomena, and on a deterministic function of the distance and the frequency. As it is shown in (7), in general, the channel presents a different response to each link. It could be also reasonable to consider a different channel distortion $h_{\text{dist}}^{(k)}(t)$, as it is commented in Section 3. Several models have been proposed for the amplitude and delay estimation, as [18] or [19]. One of the commonly agreed points is that the duration of the multipath response for narrow pulses (1-2 nanoseconds or less) in a typical office or residential environment is between 125–200 nanoseconds depending on the building size and structure.

The channel also introduces noise and interference to the signal. The noise $n(t)$ can be modeled as additive white Gaussian noise (AWGN) with a PSD defined as $N_0/2$ whereas the interference depends on the existence of other electromagnetic signals at the same frequency band. Without taking interference into consideration, the received signal in a system with N_u transmitters will be

$$r(t) = \left[\sum_{k=1}^{N_u} s^{(k)}(t) * h^{(k)}(t)\right] + n(t) \tag{8}$$

or equivalently

$$r(t) = \left[A \sum_{k=1}^{N_u} \sum_{l=1}^{L} \sum_{j=-\infty}^{\infty} a_j^{(k)} \beta_l^{(k)} \theta\left(t - jT_f - c_j^{(k)} T_c - d_j^{(k)} \lambda - \tau_0^{(k)} - \tau_l^{(k)}\right)\right] + n(t). \tag{9}$$

2.3. Receiver structure

The UWB receiver must determine the value of sequences $\{d_j^{(k)}\}$ and $\{a_j^{(k)}\}$ based on the observation at the receiver antenna terminals of the received signal $r(t)$ in time intervals whose duration is $T_s = N_s T_f$. In order to achieve that, and providing the receiver that can estimate the channel response of the desired link, a RAKE receiver can be implemented (as

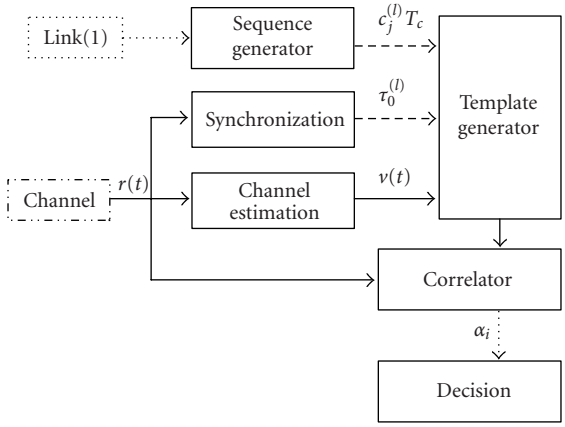

Figure 5: Conceptual model of the UWB receiver for the first user.

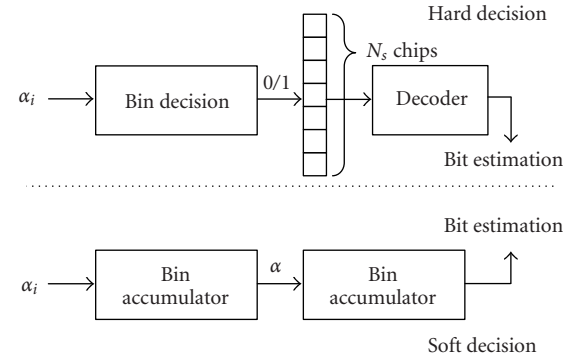

Figure 6: Hard and soft decision examples. In the hard decision (upper part), the sequence of chips is considered a codeword that is stored in a register prior to its decoding. In the soft decision (lower part), chip statistics are first accumulated in a bit statistic variable α and then the decision is taken.

the one proposed in [20]) with $L_{\max} < L$ fingers. This RAKE must be able to capture a large number of different multipath components (fingers) and combine them to improve the signal-to-noise ratio (SNR). Each one of its $L_{\max}$ fingers is adapted to a different propagation path, with two possible structures: in a *selective RAKE* (*SRAKE*), the $L_{\max}$ strongest multipath components are chosen, whereas in a *partial RAKE* (*PRAKE*), the first arriving ones are selected, yielding a less efficient (but less complex) structure. In order to simplify the receiver structure, it can be considered that the maximum duration of the RAKE fingers $\tau_{L_{\max}}^{(1)}$ is smaller than the chip period T_f, so the system is working only on two chips each time. In the vast majority of the described systems, with T_c less than two nanoseconds and low duty cycles, this condition allows the capture of most of the significant multipath components. Nevertheless, all the results shown in the following sections can be easily extended to the case $\tau_{L_{\max}}^{(1)} > T_f$.

In [21], an adaptive algorithm is presented to derive the optimal template waveform at the receiver that captures the highest amount of energy with the least number of correlations. This algorithm takes advantage of the fact that the channel effects are somehow embedded in the received signal, so the optimal template waveform can be computed based on the received signal online. Therefore, it is possible for the receiver to use a template signal adapted to the received one, providing that this kind of algorithms could be implemented.

In order to recover the information, the receiver correlates the signal $r(t)$ with the template signal, which should be previously synchronized (see Figure 5). It is necessary for the receiver to know the TH sequence of its transmitter. The statistic for the ith chip is

$$\alpha_i = \int_{iT_f+\tau_0^{(1)}+c_i^{(1)}T_c}^{(i+1)T_f+\tau_0^{(1)}+c_i^{(1)}T_c} r(t) \times v\left(t - iT_f - \tau_0^{(1)} - c_i^{(1)} T_c\right) dt, \quad (10)$$

where

$$v(t) = \sum_{m=0}^{L_{\max}} \beta_m^{(1)} \varphi\left(t - \tau_m^{(1)}\right). \quad (11)$$

The signal $\varphi(t)$ changes depending on the type of modulation employed. For PAM modulations, it is

$$\varphi(t) = \tilde{\theta}(t) \quad (12)$$

and it is

$$\varphi(t) = \tilde{\theta}(t) - \tilde{\theta}(t - \lambda) \quad (13)$$

for binary PPM (this is the one considered in the text, although extensions to M symbols can be easily achieved), where $\tilde{\theta}(t)$ is the estimated waveform. If both modulations are combined, $\varphi(t)$ depends on the way the information is coded, so different schemes could be employed.

Once the chip statistics have been calculated, a bit decision should be taken. Two different techniques can be applied: hard and soft decision (see Figure 6). The difference between them is that whereas in the first one, the decisions are taken independently on every chip, in the second one, all the chip statistics are added previously to be decided. In formal terms, the bit statistic α for the soft decision is [2]

$$\alpha = \sum_{i=1}^{N_s} \alpha_i. \quad (14)$$

In the hard decision, α is the most common value among the decisions of the N_s chips of a bit. This scheme is easier to implement than soft decision, but, in general, less efficient due to the loss of information, as it is commented in [22]. Nevertheless, hard decision can be combined with intrabit coding to provide better performance [15].

2.4. Comments on the previous simulators

So far an analytical model of a whole multiuser UWB communication system has been presented. In order to simulate it, a very straightforward structure could be based on a Monte Carlo simulation method, where a vector of bits is generated and transmitted through a given link. The vector of bits received after decision is compared with the original one and the BEP is estimated as the average number of errors

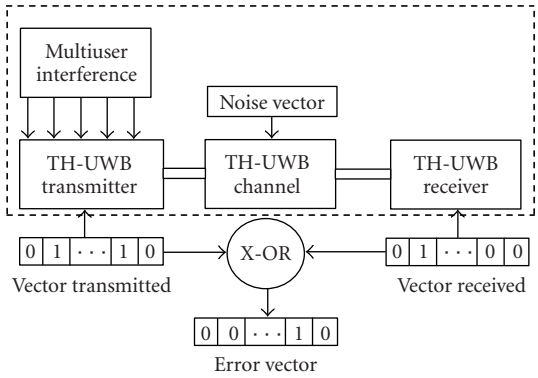

Figure 7: Simulator schematic as the one described in [8].

between the length of the vector (number of bits transmitted). In order to have a good estimation, this length should be at least two orders of magnitude greater than the inverse of the BEP [23]. Thus, hundreds of millions of bits should be processed for a BEP of 10^{-6}.

This structure is followed by the two simulators described in [8] (see Figure 7). There are two major differences between them, whereas the first one is based on a constant sampling rate and it has the same lengths for the signal and noise vectors, in the second one, only the nonzero intervals are sampled and noise is only added to those samples that have any influence on the chip statistic. The second approach provides a better performance in the case of low duty-cycle signals, as all the zero samples are ignored. Unfortunately, due to the channel multipath and the multiuser interference (MUI), the received signals present a considerable increment in the duty cycle, so in the end, both approaches present similar performances in a multiuser/multipath environment.

The main problem is the length of the vectors. For instance, a binary PPM-TH-UWB system with a bit rate of 100 kbps and 1-nanosecond pulses has ten thousands possible chip slots per bit. The necessary sampling rate to avoid aliasing can be higher than 10 gigasamples per second, depending on the waveform, so every bit is represented by at least one hundred thousand (100.000) samples. In order to simulate the different system blocks, several operations should be applied on these vectors (convolutions, windowing, etc.), so the total computing time to estimate a single BEP value for a given set of conditions can be very high, which reduces the simulator utility.

In order to improve the performance, it would be desirable to apply importance sampling methods instead of Monte Carlo. However, to do it efficiently, it is necessary for the noise to have its dimensionality close to one (the number of samples per experiment), and to have low correlation between different experiments. Therefore, the noise should be reduced to a sample per experiment with a low autocorrelation.

In the next section, a simulation structure is presented that achieves a reduction of the noise dimensionality to one and that allows an extremely fast bit processing as a consequence of the particular structure of TH-UWB signals (or, in general, of any TH signal). An additional advantage of this structure is the independence of the simulation time from the sampling rate, which can be as high as necessary without reducing the time capabilities of the system.

3. ENHANCED TH SIMULATION ALGORITHM

The aim of this section is to describe a possible enhanced structure for a TH-UWB simulator. All the results will be provided for the case of soft-decision detection, but it can be easily extended to hard decision just changing from bit simulations to chip simulations and taking into account the possible correlation between noise samples, as it will be explained in the following sections.

3.1. Signal and noise separation: signal processing

The first step is the separation between the signal and noise components of every chip statistic. Taking into consideration (9) and (10), a chip statistic α_i can be described as

$$\alpha_i = \alpha_i^s + \alpha_i^n, \tag{15}$$

where

$$\alpha_i^s = \int_{iT_f+\tau_0^{(1)}+c_i^{(1)}T_c}^{(i+1)T_f+\tau_0^{(1)}+c_i^{(1)}T_c} r^s(t) \times v\left(t - iT_f - \tau_0^{(1)} - c_i^{(1)}T_c\right)dt, \tag{16}$$

$$r^s(t) = \left[\sum_{k=1}^{N_u} s^{(k)}(t) * h^{(k)}(t)\right], \tag{17}$$

is the signal component and

$$\alpha_i^n = \int_{iT_f+\tau_0^{(1)}+c_i^{(1)}T_c}^{(i+1)T_f+\tau_0^{(1)}+c_i^{(1)}T_c} n(t) \times v\left(t - iT_f - \tau_0^{(1)} - c_i^{(1)}T_c\right)dt \tag{18}$$

is the noise contribution to the chip statistic.

It would be desirable to extract the effects related to the waveform distortion from those related to the delay in an attempt to simplify the system. It is known that given two functions $\psi(t)$ and $\xi(x)$, with $\xi(x)$ equals to zero out of the interval $[0, T]$,

$$\begin{aligned}\psi(t) * \xi(T-t)|_{t=\tau+T} &= \int_{t-T}^{t} \psi(x)\xi(T-(t-x))dx|_{t=\tau+T} \\ &= \int_{\tau}^{\tau+T} \psi(x)\xi(x-\tau)dx,\end{aligned} \tag{19}$$

which can be applied to (16):

$$\alpha_i^s = \left[\sum_{k=1}^{N_u} s^{(k)}(t) * h^{(k)}(t)\right] * v(T_f - t)|_{(i+1)T_f+\tau_0^{(1)}+c_i^{(1)}T_c}, \tag{20}$$

where $v(t)$ is zero out of the interval $[0, T_f]$ as $\tau_{L_{\max}}^{(1)} < T_f$.

Equivalently, applying (9),

$$\alpha_i^s = \left[\sum_{k=1}^{N_u}\sum_{j=-\infty}^{\infty}\sum_{l=1}^{L} a_j^{(k)}\beta_l^{(k)}\delta\left(t - jT_f - c_j^{(k)}T_c - d_j^{(k)}\lambda - \tau_0^{(k)} - \tau_l^{(k)}\right)\right] * \theta(t) * v(T_f - t)\big|_{(i+1)T_f + \tau_0^{(1)} c_i^{(1)} T_c}. \quad (21)$$

Taking into consideration (11), the last term in (23) can be expanded, after some trivial operations, as

$$v(T_f - t) = \varphi(-t) * \sum_{m=0}^{L_{\max}} \beta_m^{(1)}\delta\left(t + \tau_m^{(1)}\right) * \delta(t + T_f); \quad (22)$$

so if we define the *transmitted-distorted-received (TDR) waveform* $\Omega(t)$ as

$$\Omega(t) = \theta(-t) * \varphi(t), \quad (23)$$

then (23) can be rewritten as

$$\alpha_i^s = \sum_{k=1}^{N_u}\sum_{j=-\infty}^{\infty}\sum_{l=1}^{L}\sum_{m=0}^{L_{\max}} a_j^{(k)}\beta_l^{(k)}\beta_m^{(1)}\delta\left(t - jT_f - c_j^{(k)}T_c - d_j^{(k)}\lambda - \tau_0^{(k)} - \left(\tau_l^{(k)} - \tau_m^{(1)}\right)\right) * \Omega(T_f - t)\big|_{(i+1)T_f + \tau_0^{(1)} + c_i^{(1)} T_c}. \quad (24)$$

The TDR signal $\Omega(t)$ is very interesting. If we consider no channel distortion and perfect signal estimation, $\Omega(t)$ becomes

$$\Omega_{\text{PAM}}(t) = w_{\text{tr}}(-t) * w_{\text{tr}}(t) \quad (25)$$

for PAM modulations or

$$\Omega_{\text{PPM}}(t) = w_{\text{tr}}(-t) * w_{\text{tr}}(t) - w_{\text{tr}}(-t) * w_{\text{tr}}(t - \lambda) \quad (26)$$

for PPM, which are respectively the signal autocorrelation (for PAM) and the subtraction of the autocorrelation and its replica shifted λ (for PPM). In the case of channel distortion, if the channel-impulse response $h_{\text{dist}}(t)$ has a duration η, then the TDR will be nonzero in the interval $[-T_c - \eta, T_c + \eta + \lambda]$ ($\lambda = 0$ for PAM). Besides, if the distortion $h_{\text{dist}}(t)$ is different for every link, then there will be a different TDR $\Omega^{(k)}(t)$ for each link.

If we apply now the reciprocal change of (19) and define

$$\varepsilon_{i,j,l,m}^{(k)} = (j - i)T_f + \left(c_j^{(k)} - c_i^{(1)}\right)T_c + \left(\tau_0^{(k)} - \tau_0^{(1)}\right) + \left(\tau_l^{(k)} - \tau_m^{(1)}\right), \quad (27)$$

then we can express α_i^s as

$$\alpha_i^s = \sum_{j,k,l,m} a_j^{(k)}\beta_l^{(k)}\beta_m^{(1)}\int_0^{T_f}\delta\left(t - \varepsilon_{i,j,l,m}^{(k)} - d_j^{(k)}\lambda\right)\Omega(t)dt. \quad (28)$$

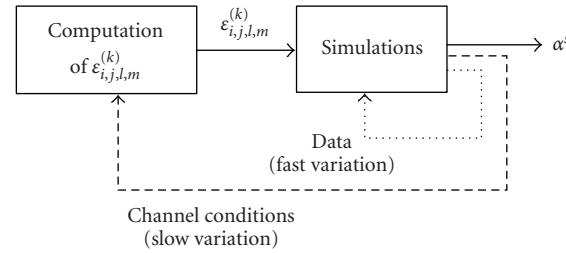

Figure 8: Signal processing flowchart. It should be noticed how $\varepsilon_{i,j,l,m}^{(k)}$ is only recomputed when the channel conditions change. The main signal simulation loop is in charge of generating data to be calculated (32).

This integral will be nonzero only for the values that satisfy

$$-d_j^{(k)}\lambda - T_c - \eta < \varepsilon_{i,j,l,m}^{(k)} < T_c + \lambda + \eta - d_j^{(k)}\lambda. \quad (29)$$

It can also be expressed with independence of the PPM transmitted data. Thus, for $i = 1, \ldots, N_s$, let $\{j, k, l, m\} \in \Gamma$ be the set of values that satisfy

$$\left|\varepsilon_{i,j,l,m}^{(k)}\right| < T_c + \eta + \lambda; \quad (30)$$

then α_i^s can be obtained as

$$\alpha_i^s = \sum_{j,k,l,m\in\Gamma} a_j^{(k)}\beta_l^{(k)}\beta_m^{(1)}\Omega\left(\varepsilon_{i,j,l,m}^{(k)} + d_j^{(k)}\lambda\right) \quad (31)$$

and the signal component of the bit statistic, in the case of soft decision detection, can be expressed as

$$\alpha^s = \sum_{i=1}^{N_s}\sum_{j,k,l,m\in\Gamma} a_j^{(k)}\beta_l^{(k)}\beta_m^{(1)}\Omega\left(\varepsilon_{i,j,l,m}^{(k)} + d_j^{(k)}\lambda\right). \quad (32)$$

As $\varepsilon_{i,j,l,m}^{(k)}$ is independent of the data, it can be computed only one time for a whole sequence of transmitted bits (see Figure 8), and so the simulation operations to evaluate (32) will be reduced, which results in a considerable time saving.

Another big difference with the "traditional" simulators is the waveform processing, based on the access at a particular TDR position given by $\varepsilon_{i,j,l,m}^{(k)} + d_j^{(k)}\lambda$, making it unnecessary to operate with the signal samples every simulation. Consequently, the sampling rate can be raised with the only penalty of increasing the TDR length, which could make the access slower. Notwithstanding, this effect is negligible as it will be tested in the next section. Therefore, it can be considered that the simulation speed is approximately independent of the sampling rate.

In the case of links with different TDR, (32) results in

$$\alpha^s = \sum_{i=1}^{N_s}\sum_{k=1}^{N_u}\sum_{j,l,m\in\Gamma^{(k)}} a_j^{(k)}\beta_l^{(k)}\beta_m^{(1)}\Omega^{(k)}\left(\varepsilon_{i,j,l,m}^{(k)} + d_j^{(k)}\lambda\right). \quad (33)$$

3.2. Noise processing

Importance sampling, as it is described in [23], allows a considerable decrease of the simulation time by reducing the number of experiments necessary to calculate a single BEP value. In order to apply importance sampling under optimum conditions, the experiments should be independent and the noise dimensionality should be close to one.

If we apply (19) to (18), the noise component α^n can be expressed as

$$\alpha^n = \sum_{i=1}^{N_s} \left[n(t) * v\left(T_f - t - iT_f - \tau_0^{(1)} - c_i^{(1)} - T_c\right)\Big|_{T_f} \right]; \tag{34}$$

so α^n is the sum of N_s samples of a filtered Gaussian stochastic process. As the interference between adjacent bits is almost negligible (it is reduced to the possible interference between the last chip RAKE and the first chip one), and α^n can be modeled as a Gaussian white process with variance σ_n^2, in the case of hard decision detection, α_i^n is also a Gaussian sequence, but its autocorrelation should be computed according to the chip interference.

To apply the importance sampling, it is just necessary to emphasize α^n standard deviation σ_n by a factor γ (whose optimum value is around 4) [23]:

$$\sigma_n^{'2} = \gamma^2 \sigma_n^2. \tag{35}$$

The new noise component $\alpha^{n'}$ should be added to the signal one α^s and the BEP of a soft decision binary system can be computed as

$$\text{BEP} = \frac{\sum_{e=1}^{N_e} \psi_e}{N_e}, \tag{36}$$

where N_e is the number of experiments (number of transmitted bits) and

$$\psi_e = \begin{cases} 0 & \text{if no error occurred in the } j\text{th experiment,} \\ w_e & \text{if an error occurred in the } j\text{th experiment,} \end{cases}$$
$$w_e = \gamma e^{(1-1/\gamma^2)(\alpha_e^{n'})^2/2\sigma_n^2}, \tag{37}$$

where $\alpha_e^{n'}$ is the emphasized noise component of the eth bit (experiment).

Whereas in the soft decision detection, the experiments are related to transmitted bits, in the hard decision, they cope with chip transmission. Once the chip error rate (CEP) is known, the BEP can be found applying the gain due to the intrachip code.

3.3. Example: PAM-TH-UWB simulator

As an example of the algorithm, we show a brief description of a PAM-TH-UWB simulator with soft decision detection. It will be a particularization of the general algorithm for the case of absence of PPM (the design of PPM or hybrid simulators is equivalent).

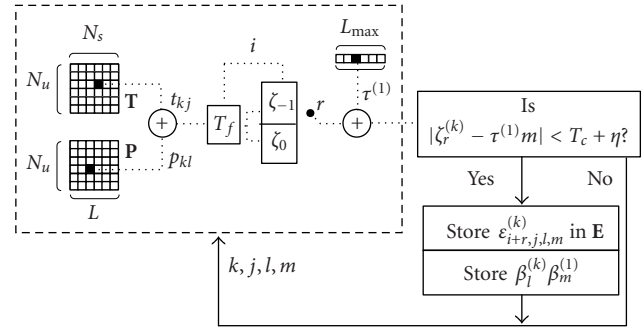

Figure 9: Matrix **E** calculation flowchart.

First of all we should define the matrices **T** (chip position) and **P** (channel delay) as

$$\mathbf{T} = \begin{bmatrix} c_1^{(1)} T_c + T_f + \tau_0^{(1)} & \cdots & c_{N_s}^{(1)} T_c + N_s T_f + \tau_0^{(1)} \\ \vdots & \ddots & \vdots \\ c_1^{(N_u)} T_c + T_f + \tau_0^{(N_u)} & \cdots & c_{N_s}^{(N_u)} T_c + N_s T_f + \tau_0^{(N_u)} \end{bmatrix},$$
$$\mathbf{P} = \begin{bmatrix} \tau_1^{(1)} & \cdots & \tau_L^{(1)} \\ \vdots & \ddots & \vdots \\ \tau_1^{(N_u)} & \cdots & \tau_L^{(N_u)} \end{bmatrix}. \tag{38}$$

In order to compute $\varepsilon_{i,j,l,m}^{(k)}$, we choose an element t_{kj} of **T** and another p_{kl} of **P** (see Figure 9), $1, \ldots, k, \ldots, N_u$, $1, \ldots, j, \ldots, N_s$, $1, \ldots, l, \ldots, L$, and we add them. The result is the position of the lth received echo of jth chip of the kth link. We can calculate i (position in the first link frame) as $\lfloor (t_{kj} + p_{kl})/T_f \rfloor$, where $\lfloor \cdot \rfloor$ denotes "the maximum integer smaller than this value." This chip affects both the ith and the $(i-1)$th receiver windows (due to the RAKE length). Thus, the two possible relative positions will be

$$\zeta_r^{(k)} = (t_{kj} + p_{kl}) - c_{(i+r)}^{(k)} T_c - (i+r) T_f, \quad r = -1, 0. \tag{39}$$

These positions affect the decision if (30) is verified; therefore we can compute all the values that satisfy $|\varepsilon_{i+r,j,l,m}^{(k)}| = |\zeta_r^{(k)} - \tau_m^{(1)}| < T_c + \eta$, $1, \ldots, m, \ldots, L_{\max}$, $r = -1, 0$, and we store them in the row vectors $\mathbf{e}^{(k)}$, with a length inferior to $2L_{\max} L N_s$. The elements of $\mathbf{e}^{(k)}$ are the values $\varepsilon_{i+r,j,l,m}^{(k)}$ that verify (30). Finally, we *define* the matrix **E** as

$$\mathbf{E} = \begin{bmatrix} \mathbf{e}^{(1)} \\ \mathbf{e}^{(2)} \\ \vdots \\ \mathbf{e}^{(N_u)} \end{bmatrix} = \begin{bmatrix} e_{11} & \cdots & e_{1Q} \\ \vdots & \ddots & \vdots \\ e_{N_u 1} & \cdots & e_{N_u Q} \end{bmatrix}. \tag{40}$$

Matrix **E** should be recalculated only when the channel conditions change. Depending on the channel coherence time and the bit rate, it is possible to find the number of bits K that can be simulated without altering **E**. The size of **E** will be $N_u \times Q$, where Q (number of components of the largest

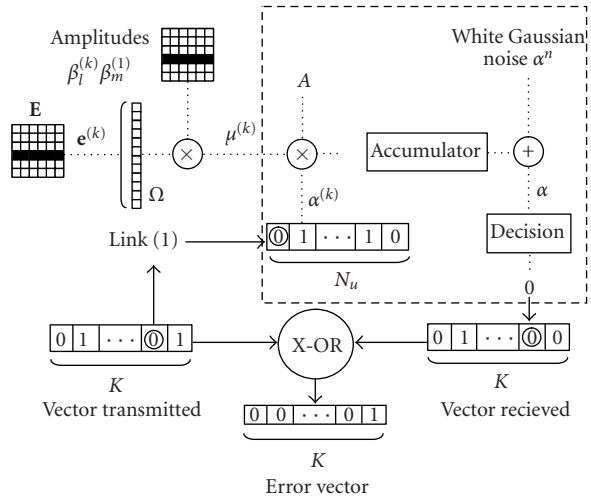

Figure 10: Error vector calculation flowchart.

$\mathbf{e}^{(k)}$) depends on the channel and RAKE structure, its average value is in general inferior to $2L_{\max}LN_s/N_u$, and in the case of no overlapping of the RAKE windows, this value is smaller than $2LN_s/N_u$. The rows whose length is less than Q are completed with zeros.

Not only are the valid $\varepsilon_{i+r,j,l,m}^{(k)}$ values stored, but also their corresponding amplitudes $\beta_l^{(k)}\beta_m^{(1)}$. It should be noticed how the algorithm complexity is linear with N_u (number of users), N_s (number of chips per bit), L (number of multipath components), and $L_{\max}$ (number of fingers), as it will be analyzed in the following section.

The second part of the algorithm develops the importance sampling simulation method, as represented in Figure 10. There it can be seen how the values stored in **E**, which represent time positions in the TDR waveform, are used to generate their correspondent values, which should be multiplied by their amplitudes and the transmitted data. Therefore, the vector **J** can be defined as

$$\mathbf{J} = A\begin{bmatrix} a^{(1)}\mu^{(1)} \\ a^{(2)}\mu^{(2)} \\ \vdots \\ a^{(N_u)}\mu^{(N_u)} \end{bmatrix} \tag{41}$$

with

$$\mu^{(k)} = \sum_{q=1}^{Q}\beta_{l_q}^{(k)}\beta_{m_q}^{(1)}\Omega(e_{kq}) = \sum_{i,j,k,l,m\in\Gamma}\beta_l^{(k)}\beta_m^{(1)}\Omega\left(\varepsilon_{i,j,l,m}^{(k)}\right). \tag{42}$$

Matrix **J** stores the information about the desired signal $Aa^{(1)}\mu^{(1)}$ and the MUI:

$$\text{MUI} = A\sum_{k=2}^{N_u}a^{(k)}\mu^{(k)}; \tag{43}$$

therefore the component α^s is the sum of both. It is important to notice how the sampling rate f_s only determines the size of $\Omega(t)$, so it has little impact on the total computing time. A is in charge of controlling the SNR, thus, given a waveform $\Omega(t)$, A can be defined as

$$A = \frac{\sqrt{\text{SNR}}}{\Omega(0)\sum_{m=1}^{L_{\max}}\left(\beta_m^{(1)}\right)^2}\sigma_n, \tag{44}$$

where σ_n is the noise standard deviation, which can be set to one. Therefore, the decision variable α is defined as

$$\alpha = \alpha^s + X, \tag{45}$$

where X is a zero-mean Gaussian random variable with variance γ^2 (emphasis factor).

4. ALGORITHM PERFORMANCE

4.1. Time performance

Speaking about time performance, three facts should be remarked:

(1) computational time grows linearly with the number of users, the number of chips, the channel length, and the number of fingers;
(2) computational time is independent of the sampling frequency;
(3) the total simulation time per bit is steadily reduced as the SNR (and consequently the number of simulations per bit) increases.

The first statement can be seen in Figure 11, with the representation of the computational time per bit in relation to the number of chips and to the number of multipath components. A linear behavior that is equivalent to the number of users and the number of fingers can be seen, which is due to the simulator structure.

The effect of the sampling frequency on time performance can be seen in Figure 12. There it is shown how there is no dependence between the bit simulation time and the sampling frequency. Therefore, a very high accuracy can be obtained without affecting the simulation time, which is a very important feature of the algorithm, and which can be easily extended to other communication system simulators.

In Table 1, a comparison of simulation times per bit as the SNR grows under a fixed set of conditions (T_c = 1 nanosecond, N_h = 32 slots, N_u = 1 link, λ = 180 picoseconds, L = 500 paths, N_s = 1, and $L_{\max}$ = 1 finger) is presented. A steady reduction in the computational time per bit for the enhanced simulator can be seen. As it was commented in the previous section, the evaluation of **E** consumes a fixed time independently of the number of simulations. The higher the SNR is, the lower the BEP is, and so a larger number of simulations are required. Therefore, the fixed time is distributed among a bigger number of bits and, consequently, its influence on the bit time is smaller.

All the simulations have been done in Matlab with a Pentium IV 1600 MHz with 128 MHz RAM.

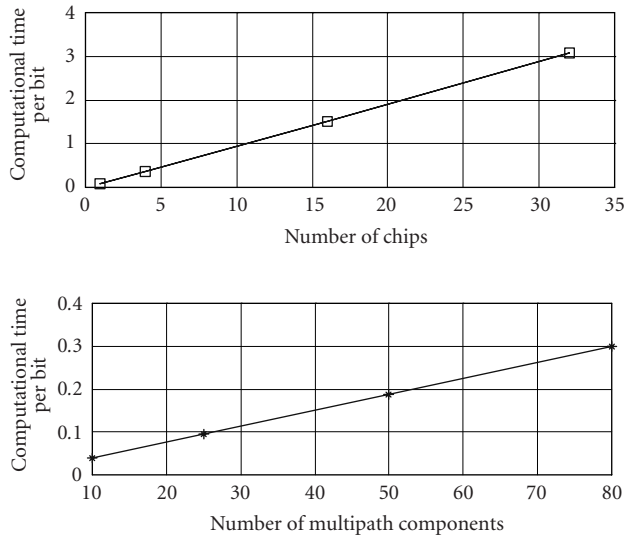

Figure 11: Computational time (per bit) for a PPM-TH-UWB system with $T_c = 1$ nanosecond, $N_h = 1024$ slots, $N_u = 50$ links, $f_s = 200\,\text{GHz}$, $\lambda = 180$ picoseconds, and $L_{\max} = 10$ fingers. In the upper one, L is set to 100 paths and in the lower one, N_s is 4 chips/bit.

In Table 2, the simulation times per bit of the two simulators presented in [8] are shown under equivalent parameters (N_h, L, etc.). The platforms where the simulations were done are unknown, so there is no possible comparison with Table 1. However, it should be noticed that the times presented in [8] are constant with the SNR, so the total time will grow exponentially with the SNR. It is also important to remark that only two years separate between [8] and this paper, but the time performance has been improved by more than two orders of magnitude.

4.2. Comparison with theoretical results

In (47), a theoretical analysis of the performance of a PPM-TH-UWB systems under certain restrictions is presented, based on the one presented in [2] by Win and Scholtz. In order to validate the algorithm, we have decided to test the numerical results against the theoretical response. This analysis does not take into consideration explicitly neither the multipath characteristics of the channel nor the RAKE structure—only the signal distortion (where the multipath could be embedded). Under the assumptions of independent links and random sequence selections (with $C_{\max} < N_h/2$), the MUI can be modeled as Gaussian and the BEP for soft decision can be expressed as

$$\text{BEP} = Q\left[\sqrt{\text{SNR}\,(N_u)}\,\right], \tag{46}$$

$$\text{SNR}\,(N_u) = \frac{\left(A^{(1)} N_s \int_{-\infty}^{\infty} \theta(t)\varphi(t)dt\right)^2}{\sigma_n^2 + \sum_{k=2}^{N_u} \left(A^{(k)}\right)^2 (N_s/T_f) \int_{-\infty}^{\infty} \left[\int_{-\infty}^{\infty} \theta(t-s)\varphi(t)dt\right]^2 ds}, \tag{47}$$

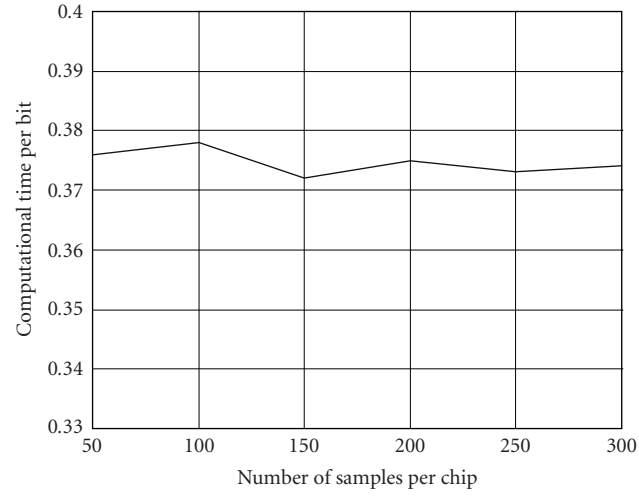

Figure 12: Effect of the sampling rate on the computational time (per bit) for a PPM-TH-UWB system with $T_c = 1$ nanosecond, $N_h = 1024$ slots, $N_u = 50$ links, $\lambda = 180$ picoseconds, $L = 100$ paths, $N_s = 4$, and $L_{\max} = 10$ fingers.

Table 1: Simulation times per bit for the simulation chain described in this paper.

SNR	Enhanced
4	0.0039 s
5	0.0016 s
6	0.0009 s
7	0.0005 s
8	0.0003 s

Table 2: Comparison of simulation times per bit for the simulation chains presented in [8].

SNR	Fixed rate	Variable rate
4	0.2434 s	0.0863 s
5	0.2428 s	0.0863 s
6	0.2427 s	0.0860 s
7	0.2425 s	0.0862 s
8	0.2354 s	0.0863 s

where

$$Q(x) = \frac{1}{\sqrt{2\pi}} \int_x^{\infty} e^{-y^2/2} dy. \tag{48}$$

Equation (47) can be equivalently expressed as

$$\text{SNR}\,(N_u) = \left(\frac{1}{\text{SNR}(1)} + \frac{1}{N_s T_f \Omega(0)^2} \sum_{k=2}^{N_u} \left(\frac{A^{(k)}}{A^{(1)}}\right)^2 \int_{-\infty}^{\infty} [\Omega(s)]^2 ds\right)^{-1}, \tag{49}$$

where SNR(1) is the signal-to-noise ratio in the single-user case (without MUI). In Figure 13, it can be seen how the assumption of a Gaussian distribution of the MUI is valid under the assumption of no multipath response. It yields the

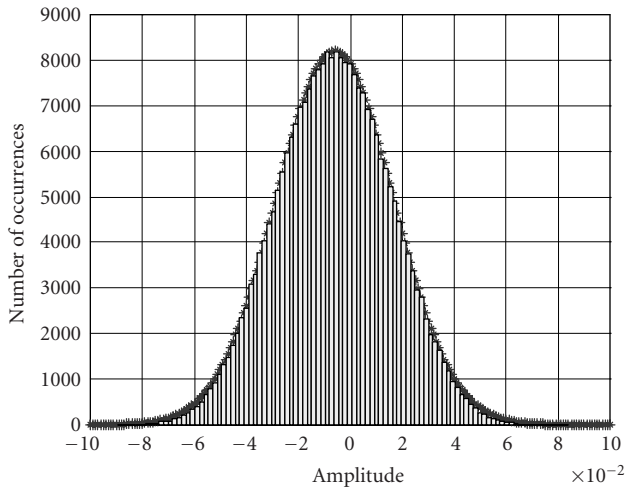

Figure 13: Histogram of the distribution of the MUI for a PPM-TH-UWB system with $T_c = 1$ nanosecond, $N_h = 1024$ slots, $N_u = 900$ links, $\lambda = 180$ picoseconds, $N_s = 64$, and no multipath. The number of simulations is 330.503. The Gaussian distribution of the interference can be noticed. The theoretical Gaussian envelope can be seen, with a mean value of 0.006 and a standard deviation of 0.0225.

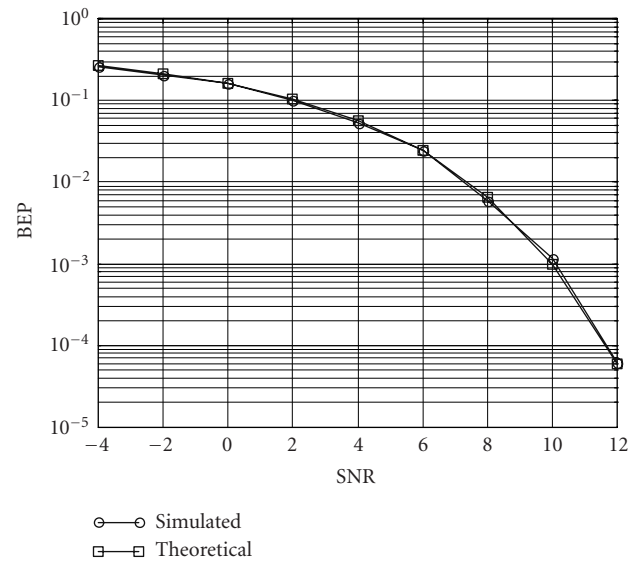

Figure 14: Comparison between the simulated response and the theoretical response (47) for a PPM-TH-UWB system with $T_c = 1$ nanosecond, $N_h = 1024$ slots, $N_u = 900$ links, $\lambda = 180$ picoseconds, $N_s = 64$, and no multipath. The number of simulations per point for SNR = 10 and 12 was one order of magnitude higher than the expected BEP.

performance shown in Figure 14. It is important to remark that for BEP lower than the inverse of the number of simulations, divergences between the theoretical and simulated responses may appear in the high SNR region of the graphic (right-hand side).

These divergences are due to the fact that the importance sampling only optimizes the number of simulations in the left region, where the noise interference is the main cause of errors. Thus, when the MUI is larger than the noise interference, it is necessary to increase the number of simulations to the equivalent of a situation without importance sampling to avoid such divergences.

4.3. Theoretical performance in a multipath environment

The theoretical model previously commented works properly in the absence of multipath propagation, but does not explicitly include the multipath channel response or the RAKE structure. Thus, the simulator presented can be employed, for example, to validate an extension of this model, as the one presented by us in (50). The development is simple. On one hand, the L paths of each link can be modeled as $(N_u - 1)L$ independent sources, with amplitudes $\beta_l^{(k)}$. On the other hand, the template waveform changes from $\varphi(t)$ to $\sum_{m=1}^{L_{\max}} \beta_m^{(1)} \varphi(t - \tau_m^{(1)})$. If we calculate the average values for the MUI, we get

$$\mathrm{SNR}\,(N_u) = \left(\frac{1}{\mathrm{SNR}(1)} + \frac{\tilde{\beta}_{\mathrm{RAKE}}^2 L \sum_{k=2}^{N_u} \chi_{\mathrm{channel}(k)}^2}{N_s T_f L_{\max} \chi_{\mathrm{RAKE}}^2 \Omega(0)^2} \int_{-\infty}^{\infty} [\Omega(s)]^2 ds \right)^{-1}, \tag{50}$$

where $\chi_{\mathrm{channel}(k)}^2$ is the mean square value of the amplitude coefficients of the kth channel-impulse response, and $\tilde{\beta}_{\mathrm{RAKE}}$ and χ_{RAKE}^2 are, respectively, the mean and the mean square values of the RAKE coefficients of the first link receiver. If no statistical channel description is available, these values can be easily estimated as

$$\begin{aligned} \hat{\chi}_{\mathrm{channel}(k)}^2 &= \frac{1}{L} \sum_{l=1}^{L} \left(\beta_l^{(k)} \right)^2, \\ \hat{\tilde{\beta}}_{\mathrm{RAKE}} &= \frac{1}{L_{\max}} \sum_{m=1}^{L_{\max}} \beta_m^{(1)}, \\ \hat{\chi}_{\mathrm{RAKE}}^2 &= \frac{1}{L_{\max}} \sum_{m=1}^{L_{\max}} \left(\beta_m^{(1)} \right)^2. \end{aligned} \tag{51}$$

The empirical validation of (50) is shown in Figure 15. There it can be seen how (50) describes accurately the system performance.

There are several approaches where the simulator can be very useful, including the possibility of optimization by simulation, where given a set of constraints, a parameter is optimized by simulating its performance and finding the optimum value. This can be achieved thanks to the algorithm speed.

5. CONCLUSIONS

Under a linear description of a TH system with a multipath channel, it is possible to reduce the simulation process to a series of arithmetical operations, avoiding any filtering or convolutions, which are operations that consume a great amount

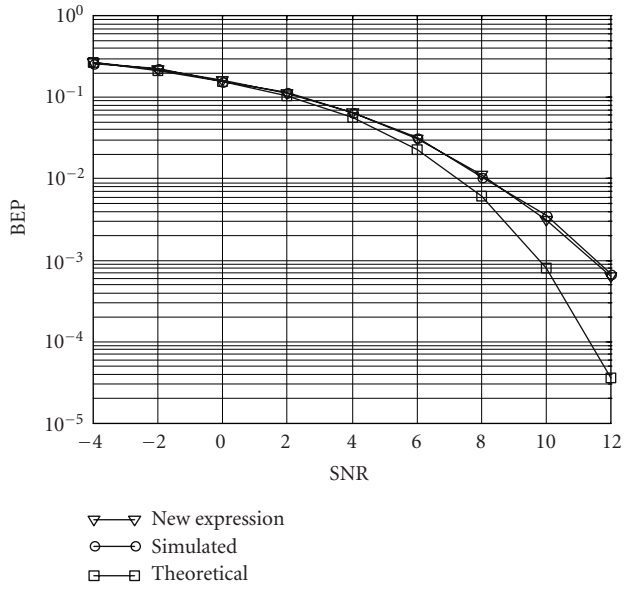

Figure 15: Comparison between the simulated response and the two theoretical expressions (the one denoted as "theoretical" is based on Scholtz's formula (47), and "new expression" is the formula presented in this paper in (50)) for a PPM-TH-UWB system with $T_c = 1$ nanosecond, $N_h = 1024$ slots, $N_u = 300$ links, $\lambda = 180$ picoseconds, $N_s = 16$, $L = 80$, and $L_{\max} = 10$ fingers. It can be seen how (50) describes exactly the behavior of the simulated response.

of computational time. Following this philosophy, in this paper, an algorithm to design TH-UWB simulators has been outlined and its performance has been tested.

As an example of the simulator utility, an improved theoretical equation of the performance of TH-UWB systems in the presence of multipath distortion has been proposed and validated thanks to the simulated response. Besides, there are several possible applications of the simulator, from code testing to optimization by simulation, which can be explored in the future. It is also interesting to notice the possibility, mentioned in the text, of combining PAM and PPM modulations to achieve not a higher data rate, but a greater randomness that yields a lower spectral density by reducing its peaks. As spectral control is a critical issue in the development of UWB systems, this can be an interesting approach, instead of a reduction of the transmitted power.

ACKNOWLEDGMENTS

The authors would like to thank Mr. Iker Almandoz and Mr. Jon Berakoechea for their reviews and comments on the text. They also thank Mr. Javier Jiménez Leube from the Universidad Politécnica de Madrid and Mr. Fernando Mojica from École Polytechnique de Montréal for their support and encouragement.

REFERENCES

[1] M. Z. Win, J. Ju, X. Qiu, V. O. K. Li, and R. A. Scholtz, "ATM based ultra-wide bandwidth multiple-access radio network for multimedia PCS," in *Proc. IEEE 4th Annual Networld+Interop Conference*, pp. 101–108, Las Vegas, Nev, USA, May 1997.

[2] M. Z. Win and R. A. Scholtz, "Ultra-wide bandwidth time-hopping spread-spectrum impulse radio for wireless multiple-access communications," *IEEE Trans. Commun.*, vol. 48, no. 4, pp. 679–689, 2000.

[3] M. Z. Win and R. A. Scholtz, "Impulse radio: how it works," *IEEE Communications Letters*, vol. 2, no. 2, pp. 36–38, 1998.

[4] Federal Communications Commission (FCC), "Revision of Part 15 of the commission's rules regarding ultra wideband transmission systems," First Report and Order, ET Docket 98–153, April 2002, FCC 02-48, Adapted: February Released: April 2002.

[5] J. T. Conroy, "Spectral characteristics of monopulse communication signals," M.S. thesis, Department of Electrical and Computer Engineering, Illinois Institute of Technology, Chicago, Ill, USA, 1997.

[6] C. Razzell, D. Birru, B. Redman-White, and S. Kerry (Philips), "An alternate high-rate PHY for wireless personal area networks," IEEE 802.15-03/125r2, March 2003.

[7] G. Shor (Wisair), "UWB multiband alternate physical layer for TG 802.15.3a," IEEE 802.15-03/151r3, May 2003.

[8] Whyless Project, "Air interface concept (including channel model)," IST-2000-25197, Deliverable D5.1, January 2002.

[9] F. Ramirez-Mireles, "Performance of ultrawideband SSMA using time hopping and M-ary PPM," *IEEE J. Select. Areas Commun.*, vol. 19, no. 6, pp. 1186–1196, 2001.

[10] J. T. Conroy, J. L. LoCicero, and D. R. Ucci, "Communication techniques using monopulse waveforms," in *Proc. IEEE Military Communications Conference Proceedings (MILCOM '99)*, vol. 2, pp. 1181–1185, Atlantic City, NJ, USA, October–November 1999.

[11] X. Chen and S. Kiaei, "Monocycle shapes for ultra-wideband system," in *Proc. IEEE Int. Symp. Circuits and Systems (ISCAS '02)*, vol. 1, pp. 1579–1600, Scottsdale, Ariz, USA, May 2002.

[12] M. S. Iacobucci and M.-G. Di Benedetto, "Time hopping codes in impulse radio multiple access communication systems," in *Proc. International Workshop on 3G Infrastructure and Services*, pp. 171–175, Athens, Greece, July 2001.

[13] J. Romme and L. Piazzo, "On the power spectral density of time-hopping impulse radio," in *Proc. IEEE Conference on Ultra Wideband Systems and Technologies (UWBST '02)*, pp. 241–244, Baltimore, Md, USA, May 2002.

[14] M. Z. Win, "On the power spectral density of digital pulse streams generated by M-ary cyclostationary sequences in the presence of stationary timing jitter," *IEEE Trans. Commun.*, vol. 46, no. 9, pp. 1135–1145, 1998.

[15] A. R. Forouzan, M. Nasiri-Kenari, and J. A. Salehi, "Performance analysis of ultrawideband time-hopping code division multiple access systems: uncoded and coded scheme," in *Proc. IEEE International Conference on Communications (ICC '01)*, vol. 10, pp. 3017–3021, Helsinki, Finland, June 2001.

[16] D. Cassioli, M. Z. Win, and A. F. Molisch, "The ultra-wide bandwidth indoor channel: from statistical model to simulations," *IEEE J. Select. Areas Commun.*, vol. 20, no. 6, pp. 1247–1257, 2002.

[17] J. Kunisch and J. Pamp, "Measurement results and modeling aspects for the UWB radio channel," in *Proc. IEEE Conference on Ultra Wideband Systems and Technologies (UWBST '02)*, pp. 19–24, Baltimore, Md, USA, May 2002.

[18] A. Alvarez, G. Valera, M. Lobeira, R. P. Torres, and J. L. García, "UWB channel model contribution from ACORDE and University of Cantabria," in *21st Meeting of the IEEE 802.15 SG3a*, Koloa, Hawaii, USA, November 2002.

[19] J. Foerster and Q. Li, "UWB channel modeling contribution from Intel," IEEE P802.15-02/279r0-SG3a, June 2002.

[20] D. Cassioli, M. Z. Win, F. Vatalaro, and A. F. Molisch, "Performance of low-complexity RAKE reception in a realistic UWB channel," in *Proc. IEEE International Conference on Communications (ICC '02)*, vol. 2, pp. 763–767, April–May 2002.

[21] A. Taha and K. M. Chugg, "On designing the optimal template waveform for UWB impulse radio in the presence of multipath," in *Proc. IEEE Conference on Ultra Wideband Systems and Technologies (UWBST '02)*, pp. 41–45, Baltimore, Md, USA, May 2002.

[22] G. D. Weeks, J. K. Townsend, and J. A. Freebersyser, "Performance of hard decision detection for impulse radio," in *Proc. IEEE Military Communications Conference Proceedings (MILCOM '99)*, vol. 2, pp. 1201–1206, Atlantic City, NJ, USA, October–November 1999.

[23] M. C. Jeruchim, P. Balaban, and K. S. Shanmugan, *Simulation of Communication Systems*, Plenum Press, New York, NY, USA, 1992.

Galo Nuño-Barrau received the Telecom Engineer degree (*summa cum laude*) from Universidad Politécnica de Madrid (UPM), Spain, in 2002. He is currently working toward the Ph.D. degree at the Signal Processing Group of this university. He was employed as a Research Assistant in the Department of Electrical Engineering, UPM, from 2001 to 2002, working on various problems in signal processing and simulation. During 2002–2003, he was researching on substrate integrated waveguide technology under the supervision of Professor Ke Wu at Polygrames Research Center, École Polytechnique de Montréal, Montréal, Québec. He has been awarded a Telefónica Móviles Fellowship, a Rafael Escolá Prize, and the ETSIT-UPM Special Award to the best academic trajectory. He is currently working as an Associate Consultant at The Boston Consulting Group, where he focuses on business analysis and strategic consulting. His research interests include UWB systems, ad hoc networks, and wireless communications.

José M. Páez-Borrallo received the Telecom Engineer and the Doctor Engineer degrees from Universidad Politécnica de Madrid (UPM), Spain, in 1982 and 1987, respectively. From 1982 to 1985, he was with AEG-Telefunken (Ulm, Germany, and Madrid, Spain) as a Project Engineer. From 1986 to September 1987, he was with Electrónica ENSA as a Project Manager. In both companies, he was involved in the development of radiocommunications and signal classification systems for the Spanish Army. He joined the UPM as a faculty staff member in September 1987, first as an Associate Professor until July 1998 and then as a Full Professor. From 1999 to 2000, he was a Visiting Researcher at International Computer Science Institute (ICSI) and Berkeley Wireless Research Center (BWRC) at Berkeley, Calif, USA. He also served as an Academic Secretary in the Departamento de Señales, Sistemas y Radiocommunicaciones, UPM, from 1994 to 1998, and he is presently the Head of the Escuela Técnica Superior de Ingenieros de Telecomunicación (ETSIT). His main research activities are in the area of signal processing with special emphasis on the fields of communications and audio.